J Mol Model (2012) 18:4225–4237
DOI 10.1007/s00894-012-1408-1

ORIGINAL PAPER

Exploring hydrogen bond in the excited state leading toward intramolecular proton transfer: detailed analysis of the structure and charge density topology along the reaction path using QTAIM

Sivaprasad Mitra · Asit K. Chandra · Pynsakhiat Miki Gashnga · Samantha Jenkins · Steven R. Kirk

Received: 3 February 2012 / Accepted: 16 March 2012 / Published online: 4 May 2012

Abstract Excited state intramolecular proton transfer (ESIPT) reaction along the O-H····O hydrogen bond of *o*-hydroxy benzaldehyde (OHBA), methyl salicylate (MS) and salicylic acid (SA) was investigated by *ab-initio* quantum chemical calculation and theory of atoms and molecules (QTAIM) for the first time. Variation in several geometric as well as QTAIM parameters along the reaction coordinate was monitored in the fully relaxed excited state potential energy curve (PEC) obtained from intrinsic reaction coordinate (IRC) analysis. Although, the excited state barrier height for the forward reaction ($\Delta E_0^{\#}$) reduces substantially in all the systems, MS and SA do not show any obvious asymmetry for proton transfer. For MS and SA, the crossover of the bond index as well as the lengths of the participating bonds at the saddle point is assigned due to this symmetry in accordance with bond energy – bond order (BEBO) model, which does not hold true in OHBA both in the ground and excited states. Bond ellipticity, covalent and metallic character were examined for different structures along the reaction path within the QTAIM framework. The QTAIM analysis was found to be able to uniquely distinguish between the ground and excited states of the OHBA molecule as well as both determining the effects on the bonding character of adding different substituent groups and differentiating between the ESIPT reactions in the SA and MS molecules.

Keywords *Ab-intio* calculation · Bond ellipticity · Covalent and metallic character · ESIPT · Intramolecular hydrogen bond · IRC analysis · QTAIM

Introduction

Weller [1–3] was the first to propose an intramolecular proton transfer reaction in the excited state (ESIPT) to account for the unusually large Stokes-shift in the fluorescence properties of methyl salicylate (MS, Scheme 1) parent molecule. Since this first observation and its subsequent explanation, the field of ESIPT reactions has been expanding rapidly due to its potential application in different areas of science and technology [4–14].

ESIPT usually involves probing of six membered rings with an intramolecular hydrogen bond; though, the involvement of five as well as seven membered ring systems has also been observed [15, 16]. ESIPT molecules are normally stable in the enol form (**E**) in the ground state but in the tautomer (keto) form (**K***) in the excited state; therefore, such molecular systems can undergo four-level cyclic proton transfer reactions as depicted in Scheme 1. Thus, the absorption from **E** → **E*** and the emission from **K*** → **K** result in an exceptionally and anomalously large Stoke's shift. However, sometimes the normal **E*** → **E** emission is also observed along with the ESIPT emission. Normally, the proton moves between two hetero

Electronic supplementary material The online version of this article (doi:10.1007/s00894-012-1408-1) contains supplementary material, which is available to authorized users.

S. Mitra (✉) · A. K. Chandra · P. M. Gashnga
Department of Chemistry, North-Eastern Hill University, Shillong 793 022, India
e-mail: smitra@nehu.ac.in

S. Jenkins (✉) · S. R. Kirk
College of Chemistry and Chemical Engineering, Hunan Normal University, Changsha, Hunan 410081, China
e-mail: samanthajsuman@gmail.com

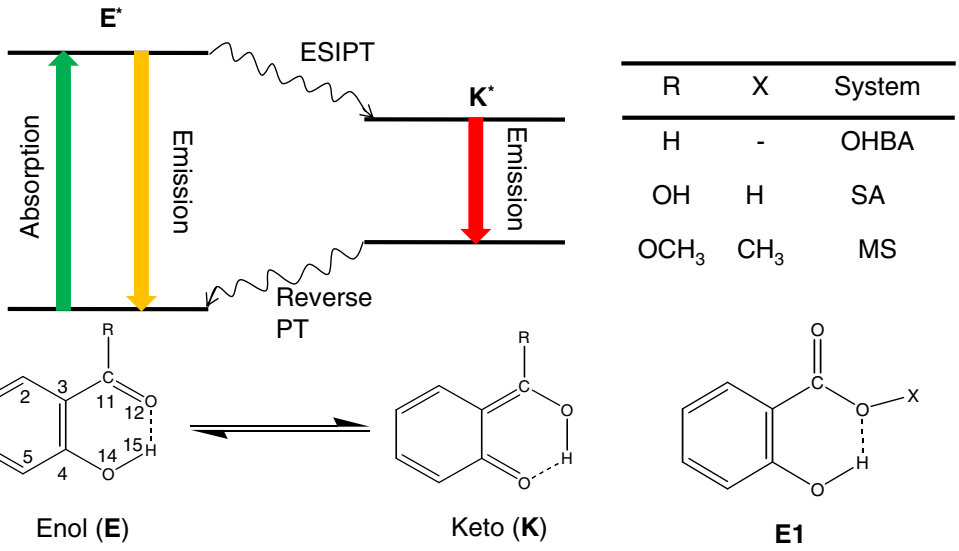

Scheme 1 Schematic energy level diagram for a cyclic four level ESIPT system. Also shown are the structures of different possible conformers for the investigated systems along with the numbering scheme used in the calculation

atoms of the type –O-H·····O, –N-H·····O, –S-H·····O etc. Due to its intramolecular character, ESIPT can be investigated under well defined conditions and it can be directly initiated by absorption of photons from an ultra-short laser pulse. Photon absorption causes a rapid change in the electron density distribution within the molecule in the excited state resulting ESIPT. In addition, ESIPT allows studying the basic features of a chemical reaction, i.e., bond fission and formation in a comparatively simple situation.

ESIPT reactions are characterized by double well potential energy surface (PES), where the reactant stays in one side and the product (photo-tautomer) on the other [17–19]. Depending on the barrier height between these stationary points, ESIPT reactions may proceed either as proton tunneling or as a part of intramolecular vibrational redistribution (IVR) in a barrierless adiabatic potential. Indication of proton tunneling could be observed by kinetic isotope effect (KIE) [20–22]. The extent of KIE dependence is limited to the factors as the degree to which the reaction is nonadiabatic and characterized by tunneling through the potential barrier or if the reaction occurs by means of IVR, then the role of vibrational motions other than the O-H stretch are important. There is precedent for ESIPT that do not exhibit KIE [23, 24]. In these cases, ultra-short excitation of the initial molecules causes a vibrationally hot state, from which intramolecular relaxation caused by the change in geometrical parameters leads to the formation of the product. Overall, a significant number of experimental and theoretical results are available that discuss the mechanistic steps involved in the ESIPT process [25–27]. However, to the best of our knowledge, there is no report on several bond properties among different structures along the fully relaxed potential energy surface, particularly in the excited states even for the model ESIPT systems like *o*-hydroxy benzaldehyde (OHBA), salicylic acid (SA) and MS (Scheme 1) etc. In this report, we present the full analysis on excited state properties of these systems obtained by complete *ab-initio* geometry optimization and theory of atoms and molecules (QTAIM). Comparative study on the ground state parameters are also presented for OHBA only.

Methods

Geometry optimization and construction of reaction path

All calculations were done using Gaussian 03 program package [28]. The geometries of the ground and first singlet excited state of the primary structure (**E**) of all the systems were fully optimized with Hartree–Fock (HF) and configuration interaction singles-excitation (CIS) method, respectively, using the split-valence Gaussian basis set with polarization and diffused function 6-311++G(d,p) following the numbering scheme given in Scheme 1. Frequency calculation in each case was done to confirm the stationary point. All real frequencies have confirmed the presence of the local minimum, while one imaginary frequency indicated the existence of a transition state.

The IRC calculation was performed using mass-weighted internal coordinate with a step-size of 0.1 amu$^{1/2}$-Bohr, as implemented in the Gaussian 03 program. Then five points were selected on each side of TS in the reaction profile to cover the entire reaction path for the formation of **E** to **K**.

The rate constant for proton transfer (κ_H) at temperature T was estimated using the conventional transition state theory (TST) equation [29]:

$$k_H(T) = \Gamma(T)\frac{k_B T}{h}\frac{q_{TS}(T)}{q_S(T)}e^{-\Delta E_0^{\#}/RT}, \quad (1)$$

where, q_{TS} and q_S represent the partition function for the transition state (TS) for proton transfer and the species S (OHBA, MS or SA), respectively; k_B is the Boltzmann constant, $\Delta E_0^{\#}$ is the barrier height including zero point energy. The $\Gamma(T)$ is the correction factor for tunneling, since tunneling is an important factor for proton transfer reaction. The tunneling correction was estimated by using the Eckart's unsymmetric barrier method [30]. The details of this procedure can be found elsewhere [31]. The partition functions were calculated using the harmonic oscillator-rigid rotator model.

QTAIM calculation protocol and definition of different parameters

QTAIM [32] is an extension of quantum mechanics to subdomains which define an atom as an open system and provides a powerful method for the study of bonding using only the charge density distribution $\rho(\mathbf{r})$. QTAIM is well suited to returning a rich quantitative description of complex and strained bonding environments [33]. No assumptions are made about the stability or topology of the bonding interactions of the atoms within molecules since there are a set of consistent descriptors that can determine such properties without bias. We can identify critical points in the charge density distribution where $\nabla\rho(\mathbf{r})=0$, and further classify these points according to the properties of the Hessian matrix (the matrix of partial second derivatives of F(r) with respect to the components of r) evaluated at these points. Diagonalizing this matrix gives the coordinate invariant (ordered) eigenvalues $\lambda_1<\lambda_2<\lambda_3$, and the critical points are conventionally labeled using the notation (ω, σ) where ω is the rank (the number of distinct eigenvalues) and σ is the signature (the algebraic sum of the signs of the eigenvalues). In three dimensions, there are four types of topologically stable critical points; these are denoted as (3,-3) [a local maximum, usually corresponding to a nuclear position (NCP)], (3,-1) and (3,+1) [saddle points, called bond critical points (BCP) and ring critical points (RCP), respectively], and (3,+3) [cage critical points (CCP)]. We also define a piecewise continuous gradient path by evaluating $\nabla\rho$ at some point, then following this vector for an extremely small distance and evaluating $\nabla\rho$ again. In the limit of an infinitely small step, the path is continuous and corresponds to the true gradient path. The pair of special gradient paths linking a BCP with two nuclei and along which ρ is a maximum with respect to any neighboring path is known as an atomic interaction line (AIL). A bond-path is then said to exist between two nuclei linked by an AIL when the forces on the nuclei vanish (i.e., the structure is in equilibrium or geometrically optimized). QTAIM therefore provides a universal definition of what constitutes bonding; if a bond-path exists between two nuclei, they are considered to be bonded.

Closed shell interactions (e.g., ionic bonds and hydrogen bonds) are characterized by positive values of $\nabla^2\rho(\mathbf{r}_b)$, low $\rho(\mathbf{r}_b)$ values (< 0.1 au), and values of $|\lambda_1|/\lambda_3<1$; these types of interactions are dominated by the contraction of charge away from the BCP toward each of the nuclei. Conversely, shared interactions (e.g., covalent bonds) have negative $\nabla^2\rho(\mathbf{r}_b)$ values, high values of $\rho(\mathbf{r}_b)$, and values of $|\lambda_1|/\lambda_3>1$. The larger the value of $|\lambda_1|/\lambda_3$ at a BCP, the 'softer' or fuzzier a bond is. This idea of bond softness is related to metallic character, so the softer a bond the more metallic it is [34]. The inequality $|\lambda_1|/\lambda_3<1$ holds for all closed shell bonding interactions, and $|\lambda_1|/\lambda_3$ is related to the rigidity of the bond path.

We can also define an ellipticity

$$\varepsilon = |\lambda_1|/\lambda_2 - 1 \tag{2}$$

as a measure of the relative accumulation of charge in the two directions $\underline{\mathbf{e_1}}$ and $\underline{\mathbf{e_2}}$ perpendicular to the bond-path at a BCP. The most and least preferred directions of electron accumulation are $\underline{\mathbf{e_1}}$ and $\underline{\mathbf{e_2}}$, respectively. The ellipticity provides a measure of pi and sigma bond character; larger values (>0.1) indicate pi bond character and lower values sigma bond character [32]. The conformers we are concerned with in this work are molecular and the numbers of the four different types of three dimensional critical points are related by a fundamental theorem of topology; the Poincaré-Hopf relationship [32]:

$$n - b + r - c = 1, \tag{3}$$

where n, b, r, and c are the numbers of NCPs, BCPs, RCPs, and CCPs, respectively. Care must be taken to ensure that all of the critical points are found since it is possible that if a critical point finding algorithm misses both a BCP and an RCP from the same charge density distribution, then an apparently valid solution of (3) is possible.

In this work we are primarily interested in properties evaluated at the BCPs, e.g., the charge density evaluated at the BCP denoted by $\rho(\mathbf{r}_b)$ and the Laplacian $\nabla^2\rho(\mathbf{r}_b)$ also evaluated at the BCP. It was proposed earlier that $\rho(\mathbf{r}_b)$ for hydrogen bonds lie in the range 0.002-0.035 au and the Laplacian $\nabla^2\rho(\mathbf{r}_b)$ in the range of 0.024-0.139 au for positive $\nabla^2\rho(\mathbf{r}_b)$ [35, 36].

In order to address the issue of cooperativity in the bonding, we use the local total energy density at the BCP suggested by [37]:

$$H(\mathbf{r}_b) = V(\mathbf{r}_b) + G(\mathbf{r}_b). \tag{4}$$

Previously, one of us found that the usual strength in hydrogen bonds in ice Ih could be explained in terms of Eq. 3 [38], in agreement with experiment [39], where a degree in covalent character is indicated by $H(\mathbf{r}_b)<0$. Pauling describes the metallic bond as a partial covalent bond

between nearest neighbor atomic centers [40]. The more recent work on metallicity by Silvi *et al.* [41, 42] within the QTAIM framework is consistent with Pauling's view. In QTAIM, covalent character in a metallic bond is associated with non-negative values of the local energy density, $H(\mathbf{r}_b)$ [34, 35, 37].

In this work we consider for the first time, to the author's best knowledge, the QTAIM will be used to investigate the excited states for intramolecular proton transfer reaction in OHBA, SA and MS. Previous theoretical studies of evaluation and interpretation of QTAIM in excited states show both that the HF-cis method is appropriate for the creation of charge densities and that there is a significant difference between the ground state and first excited state in QTAIM properties [43].

Because ESIPT process involves a considerable amount of charge transfer, it is assumed that the QTAIM is particularly suited to monitor the subsequent changes in the chemical nature of the bonding. Previous studies on excited states have discovered metal to insulator transitions [44], so we thought that it would be relevant for excited states to apply the QTAIM metallicity measure, $\xi(r_b)$, previously introduced by one of us [34]:

$$\xi(r_b) = \rho(\mathbf{r}_b)/\nabla^2\rho(\mathbf{r}_b) \quad (5)$$

for $\nabla^2\rho(\mathbf{r}_b) > 0$. Where, $\xi(r_b) > 1$ for metallic BCPs.

A quantity that behaves in a rather similar manner with respect to predicting the direction of motion of atoms under stress, [45], previously used by one of us to examine the motion of hydrogen atoms [33].

Advantages of using QTAIM to study excited states include the ability to be able to follow the changing chemical character of the bonding on a bond-by-bond basis. Further to this, the metallicity, $\xi(r_b)$ gives relative values of the variation in the charge density with respect to the charge density, since the Laplacian $\nabla^2\rho(r_b)$ provides the measure of the variation of the charge density as it is a higher derivative. This means that we can get a better understanding of the unusual bonding environments that occur during ESIPT, such as closed shell or shared shell interactions with large values of the charge density $\rho(r_b)$ or very low values of the Laplacian $\nabla^2\rho(r_b)$. In other words, use of the metallicity $\xi(r_b)$ will be able to describe how the hydrogen and sigma bonds are chemically rather different due to the effects of the excited state and the ESIPT process as compared from these bond types in the ground state without the occurrence of ESIPT.

Results and discussion

Ground state ab-initio calculation for OHBA, MS and SA

As already mentioned, OHBA, SA and MS were selected for this investigation and the ground state geometries of all these compounds were fully optimized without any symmetry restrictions to find the global minimum structure. Only the enol form (**E**) was found as the most stable structure in the ground state for all of these compounds. Searches for a keto (**K**) minimum in the ground state were also undertaken. For OHBA, the **K** conformer is found to be energetically unstable by 67.3 kJ mol^{-1} compared with the **E** conformer and is also associated with a forward barrier height of 78.95 kJ mol^{-1} (see below for the details of calculating the transition state, TS and construction of reaction path). However, the optimization procedure always led directly to **E**, both in the cases of MS and SA. We, therefore, optimized the **K** structure using restricted optimization; where, the O12-H15 bond was first kept fixed at 0.96 Å while optimizing the rest of the structure and then O12-H15 bond was relaxed keeping other structural parameters fixed at their respective optimized values. In this way, the ground state energy difference between the **E** and **K** conformer of MS is found to be 90.4 kJ mol^{-1}. So, for all practical purposes, it can be concluded that, in the ground state, all the compounds exist in the hydrogen bonded enol structure (**E**). It is to be noted here for both MS and SA, alternative hydrogen bonded structure is also possible to exist (**E1** in Scheme 1). However, the ground state energy of the **E1** conformer is higher in energy by almost 13.68 and 12.38 kJ mol^{-1} for SA and MS respectively, compared to the respective **E** conformers. So, it is unlikely that even a small fraction of **E1** will exist in the ground state at room temperature. Moreover, as this conformer is not suitable for proton transfer even in the excited state, we do not consider them explicitly in our calculation.

The important geometric parameters in the vicinity of hydrogen bonding site resulting from the S_0 state optimization procedure for all the compounds are listed in Table 1 along with the available experimental results [46, 47]. Very close agreement of the calculated bond lengths and angles with the experimental values further strengthens the applicability of the calculation protocol used in the present study. The calculation also reveals perfectly planar structure for all the compounds in the ground state.

Proton transfer in ground and excited states: comparison of different parameters along the reaction path

Full optimization of the **E** and **K** forms of OHBA in the first excited singlet state reveals stability reversal in comparison with ground state. For example, in case of OHBA, $\mathbf{K}^*$ is found to be 20.1 kJ mol^{-1} more stable than the $\mathbf{E}^*$ conformer. These energy differences suggest that under normal experimental condition OHBA will be in the **E** form in the ground state; while on the other hand, **K** will be the predominant form in the S_1 state. Also, the forward barrier height associated with the ESIPT process decreases substantially. For

Table 1 Ground state geometric parameters for OHBA, SA and MS obtained by full optimization at HF/6-311++G(d,p) level of calculation.[a] The available experimental parameters are given in the parenthesis[b]

Parameters	System		
	OHBA	SA	MS
r(C3-C4)	1.4012 (1.39)	1.4000 (1.404)	1.3998
r(C4-O14)	1.3279 (1.36)	1.3278 (1.358)	1.3288
r(O14-H15)	0.9492 (1.04)	0.9492 (1.029)	0.9494
r(C3-C11)	1.4663 (1.46)	1.4721 (1.457)	1.4775
r(C11-C12)	1.1958 (1.22)	1.1971 (1.234)	1.1983
r(O12—H15)	1.9026	1.8592 (1.704)	1.8468
r(O12—O14)	2.7046	2.6619 (2.620)	2.6529
θ(C4-C3-C11)	121.45	119.72 (120.4)	119.77
θ(C3-C11-C12)	124.86	124.49 (122.9)	123.79
θ(C11-C12-H15)	99.45	100.77	101.31
θ(C3-C4-C14)	122.94	123.83 (122.7)	123.82
θ(C4-C14-C15)	110.62	110.56 (106.2)	110.30
θ(O12-H15-O14)	140.68	140.62	141.02

[a] Bond lengths (r) and angles (θ) are in Å and degree, respectively; [b] Experimental results for OHBA and SA are obtained from microwave spectroscopy [46] and single crystal x-ray diffraction pattern [47], respectively

example, in case of OHBA this value is 9.66 kJ mol^{-1}. Interestingly, the energy difference between the **E** and **K** form at the S_1 state is found to be only 1.1 and 2.1 kJ mol^{-1} for MS and SA, respectively. Thus both the forms are likely to exist in almost equal probability. It has already been reported that excitation of the **E** conformer in case of OHBA gives a large Stokes-shifted single broad fluorescence originated from the **K** structure [48, 49]. However, for both MS and SA, fluorescence emission from the $\mathbf{E}^*$ is also observed in addition to the ESIPT fluorescence (from $\mathbf{K}^*$ conformer) [1, 50]. In most of the literatures, the origin of this normal fluorescence is ascribed due to the presence and simultaneous excitation of the non-ESIPT structure **E1** from the ground state [51, 52]. However, as described in the previous section, our calculation reveals that the presence of **E1** is most unlikely in the ground state to explain the origin of normal fluorescence in MS and SA. Rather, it is more likely that the co-existence of both **E** and **K** in the excited state that plays an important role.

The calculated barrier height ($\Delta E_0^{\#} = E_{TS} - E_S$, where E_{TS} and E_S are the energies of the TS and species S including the zero point vibrational energy) of proton transfer for the formation of **K** from **E** in the excited state (S_1) of OHBA amounts to 9.66 kJ mol^{-1}, whereas the same for the ground state is found to be 67.61 kJ mol^{-1}. Thus excitation from S_0 to S_1 state results in a drastic decrease in the barrier height for proton transfer. The $\Delta E_0^{\#}$ values for MS and SA are calculated to be 11.71 and 12.55 kJ mol^{-1}. Overall, the ESIPT in all these compounds are found to be feasible both in terms of thermodynamic and kinetic criteria (Table 2). The calculated proton transfer rate constant (k_H) values using Eq. 1 at the S_1 state of OHBA, MS and SA are 2.02×10^{11}, 1.18×10^{11} and 9.18×10^{10} s^{-1}, respectively, at 298 K corresponding to the ESIPT time ca. 5~10 ps. Experimental results suggest that the ESIPT rate for intramolecularly hydrogen bonded systems vary within a few hundred of femtosecond till several picosecond [4, 53, 54]. The calculated ESIPT times are at least an order of magnitude higher. This difference might be due to the implicit higher barrier height invoked in the HF and also in the CIS calculations for the systems where massive change in electronic structure occurs after excitation, similar to those studied here [55, 56]. Also, involvement of multidimensional relaxation from vibrationally hot state as well as possibility of conical intersection, which normally are not taken into consideration in these calculations, may contribute toward this difference [57, 58]. Even, with the help of time-resolved photoelectron spectroscopy, an ESIPT time of <45 fs was predicted for OHBA [59]. On the other hand, real-time dynamics study of ESIPT process in MS using femtosecond depletion technique reveal the corresponding time to be ~60 fs [60]. Therefore, it can be concluded that, although the calculated results differ significantly from the experimental values; a qualitative pattern of the rate parameters can even be predicted from these simple calculations for a series of similar systems.

Proton transfer in ground and excited states: comparison of different parameters along the reaction path

Different geometry parameters might influence the excited state energy and geometrical reorganization in the proton-transfer process and the parameters associated with ESIPT process could exhibit changes during photo-tautomerization. To look into the details of the changes of different structural parameters, fully relaxed geometry optimization was performed for all the compounds at different points of the reaction path using intrinsic reaction coordinate (IRC) analysis.

Table 2 Energy parameters of the enol (**E**) and keto (**K**) conformers of OHBA, SA and MS in both S_0 and S_1 states[a]

System	Enol (**E**)		Keto (**K**)	
	S_0	S_1	S_0	S_1
OHBA	−418.407581	−418.221610	−418.382101	−418.230728
SA	−493.325635	−493.132386	−493.289482	−493.131502
MS	−532.355701	−532.161311	−532.319446	−532.160743

[a] Restricted optimization technique was followed for the **K** conformer of SA and MS in the S_0 state. See text for details

Figure 1 shows the excited state potential energy curve (PEC) for all the compounds. It is seen from the figure that although the barrier height is substantially low (9~12 kJ mol^{-1}) in all the cases, the energy of the terminal structures are almost same for both MS and SA in comparison with high exothermicity for ESIPT in case of OHBA as mentioned in the previous section. The fully optimized structures at each point are shown for OHBA only, as a representative case. The variation of different parameters along the reaction path for OHBA in the ground as well as in excited state is shown in Fig. 1S(A) along with the corresponding figures of excited states of MS and SA (B and C, respectively). As expected, C3-C11, C4-O14 and O12-H15 distance decreases while going from **E** to **K** structure; while, all other bond lengths in the vicinity of intramolecular hydrogen bond increases. Careful analysis of the bond length change reveals certain interesting observations. For example, C3-C4 bond distance in the **E** conformer of OHBA is almost similar (~1.40 Å) both in the ground and excited state. In the ground state, increase of O14-H15 distance by 0.03 Å toward the formation of **K** conformer corresponds to the increase in C3-C4 distance by only 0.01 Å. However, in the excited state, increase of O14-H15 distance by 0.05 Å is associated with 0.1 Å lengthening of the C3-C4 bond. Similarly C4-O14, C3-C11 and O12···H15 bonds were also seen to be very sensitive; however, this sensitivity is not pertinent in case of C11-O12 bond. Similar observation holds true for MS and SA as well. It is to be noted here that the angle O12-H15-O14 undergoes huge change (~20^0) in the transition state. Flattening of this angle associated with simultaneous reduction of O12···O14 distance points toward preferential inward motion of the light proton (H15) during the ESIPT process. Furthermore, it is also interesting to note that the neighboring bond angles of the transferring proton, viz. C4-C14-H15 and C11-O12-H15 undergoes gradual change during the conversion of **E**→**K**; while the rest of the angles are very sensitive to proton motion and show a drastic change even for a very small displacement of the proton.

To look explicitly into the nature of variation of bond orders during the ESIPT process, natural bond orbital (NBO) calculation was performed for all the structures in the reaction both in the ground and excited state. Figure 2 shows the representative example in the case of OHBA. Interestingly, the increase in O12-H15 bond order and simultaneous decrease in O14-H15 bond order does not show a cross over exactly at the TS point both in the ground as well as in the excited state. While in the ground state, the cross over occurs one step ahead in the reactant side of the TS, the same occurs one step further toward the product in the excited state. On the other hand, for SA and MS, the bond order crossover occurs exactly at the point of TS structure. Similar observations are also seen in the variation of these two bond lengths along the reaction path for all the molecules. This is contrary to the bond order conservation principle invoked in bond energy bond order (BEBO) calculation [61, 62]. However, as proposed in an earlier communication [63], the non-coincidence of the BO inflection point with the TS structure might be due to the unsymmetrical nature of the two bonds. Another point is that in the ground state, the TS is closer to **K** conformer; whereas in the S_1 state, it is closer to **E** conformer as expected from Hammond's principle. Hence the crossover in BO occurs

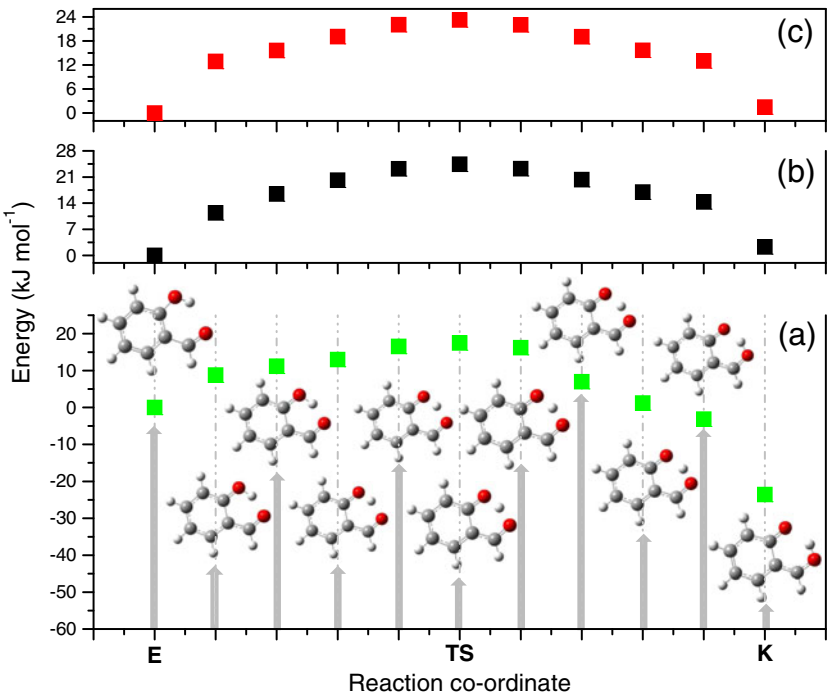

Fig. 1 Potential energy curve for the excited state enol (E) → keto (K) conversion of OHBA (**a**), SA (**b**) and MS (**c**). Fully optimized structures at different points along with the transition state (TS) are shown for OHBA only

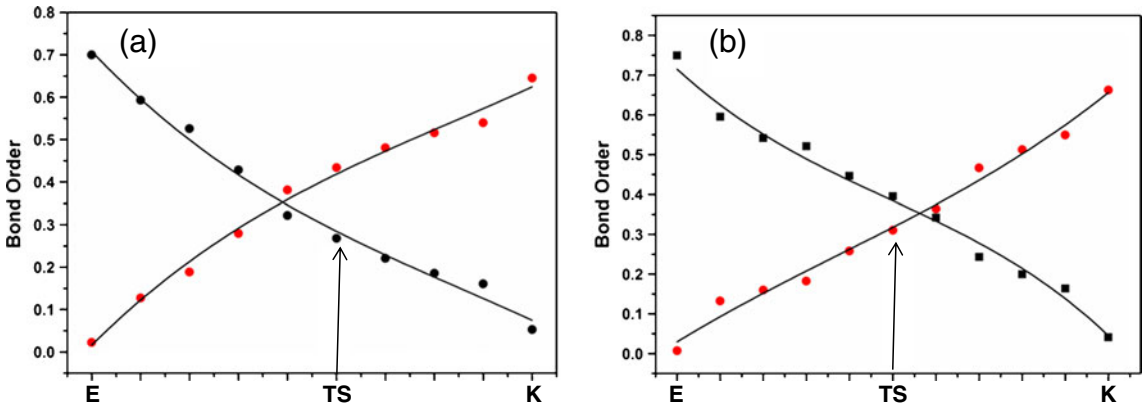

Fig. 2 Variation of bond order of O14-H15 (black dots) and O12-H15 (red dots) bonds along the reaction path in the ground (**a**) and excited (**b**) states

closer to the deeper potential and slightly before or after the energy attains it maximum value in TS, which is related to the crossover of proton from one potential well to the other. This observation further ascertains that the ESIPT occurs through somewhat more symmetric potential in both the cases of MS and SA compared with that in OHBA.

QTAIM calculation results

The results from QTAIM for the molecular graphs of different conformers of OHBA during the conversion of **E→K** in the excited states are shown in Fig. 3. The corresponding figures for SA and MS are shown in the supplement section (Figs. 2S and 3S, respectively). The four bond types which will be analyzed in this study correspond to the O14-H15, O12-H15, C11-O12 and C4-O14 bonds with the associated BCPs; BCPA, BCPB, BCPC and BCPD respectively, shown in Scheme 1. Also shown in Fig. 3a-f are the RCP-BCP as the thick gray lines. All of the QTAIM properties were calculated using AIMQB program within the AIMStudio suite [64], using the Proaim basin integration method.

In Figs. 4 and 5 as well as in 4S-5S, the **E**, **TS** and **K** label the reaction pathway coordinates. The ellipticities of the two OH bonds, namely O14-H15 and O12—H15, involved with the proton transfer and the two C-O bonds, O12-C11 and O14-C4, that attach to either end of the O-H pair, are plotted for each step of the proton transfer reaction pathway, see Fig. 4. Plots for the variation of the ellipticity (ε) and the ratio $|\lambda_1|/\lambda_3$, the covalent character H($\mathbf{r}_b$) and the metallicity $\xi(r_b)$ of the O14 -H15, O12—H15, O14-C4 and O12-C11 BCPs along the reaction pathways are presented in Figs. 4, 4S, 5S and 5, respectively. The values of these quantities do not vary significantly for any of the other bonding interactions along the reaction pathways and so were not included.

RCP-BCP paths and bond ellipticities during ESIPT

We follow the ESIPT process by examination of the changing atomic boundaries visible as the RCP-BCP paths, see Fig. 3. It can be seen that the H15 nuclei initially forms a hydrogen bond with the O12 nuclei and a covalent sigma bond with the O14 nuclei. As the H15 nuclei moves, the O12—H15 hydrogen bond shortens and the O14-H15 sigma bond lengthens until both are approximately the same length and then finally the H15 nuclei forms a hydrogen bond with the O14 nuclei and a sigma covalent bond with the O12 nuclei. The shape of the RCP-BCP paths vary during the process; those associated with the hydrogen bonds are linear the RCP-BCP lines associated with the sigma bonds are curved, with the direction of curvature toward the hydrogen bond. It is not clear why this should be the case and, to the authors' best knowledge, this phenomenon has not been investigated previously. In the mid-way along the reaction path, the two O-H BCPs possess very similar properties and the RCP-BCP lines are both curved to the same degree as can be seen in Fig. 3c. The RCP-BCP figures of the SA and MS molecules are available in the supplementary material; see Figs. 2S and 3S respectively. During passage of the H15 nuclei between the O12 and O14 nuclei, both the bond ellipticities and chemical character vary greatly as we will now describe. First we examine the effect on the ellipticity (ε), from Eq. 2, that excitation has on the proton transfer in the OHBA molecule.

The ellipticity ε of the O-H BCPs participating in the proton transfer reaction of OHBA in the excited state; O12-H15 and O14-H15 BCPs are both significantly lower than their corresponding ground state counterparts, see Fig. 4a. This is also true for the ellipticity (ε) values of the OC BCPS, O12-C11 and O14-C4, see Fig. 4b. The lower ellipticities in the excited state compared to the ground state for the OHBA molecule indicate that the bonding is less strained in the excited state, i.e., during the proton transfer

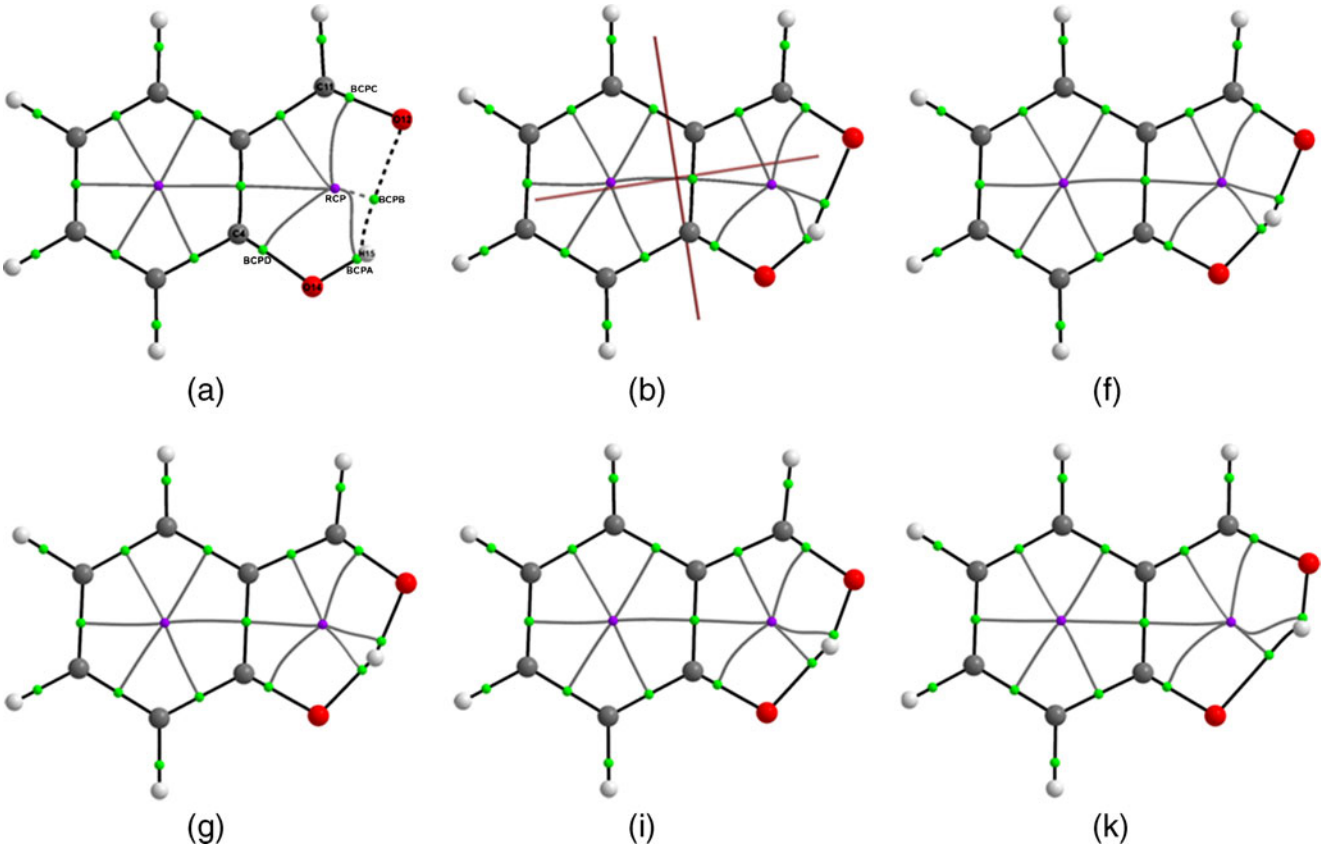

Fig. 3 The molecular graphs from QTAIM calculation of OHBA in the excited state referred to in the text are shown in sub-figures (**a**), (**b**), (**f**), (**g**), (**i**) and (**k**), the entire sequence (**a**)-(**k**) including the remaining subfigures (**c**)-(**e**) and (**h**) are given in the supplementary material, Fig. 3S. The numbering scheme that we are using is shown in sub-figure (**a**). The unmarked green and red spheres (in the electronic version) correspond to the BCPs and RCPs respectively, where the BCPs are located on the bond paths. The BCPs are labeled BCPA, BCPB, BCPC and BCPD corresponding to the O14-H15, O12-H15, O12-C11 and O14-C4BCPs, respectively. The thick gray lines indicate the positions of the RCP-BCP lines for the complete molecular graph

process. This reduction in bond ellipticity shows that the excitation of the OHBA molecule has then eased the passage of the proton along the reaction pathway in accordance with the experimental results and also *ab-initio* calculation discussed before. In addition, the reduction of the values of the ellipticities shows a change in bonding character from pi to sigma bond, values of the ellipticity of approximately 0.1 or greater indicating pi bonding character [32].

Next, we compare the effect of substituting either –OH or -OCH_3 groups corresponding to SA and MS molecules respectively, on the bond ellipticities ε. For both the SA and MS, the O12-C11 BCP usually has significantly higher values of ε than the O14-C4 BCPs; where the ε values of the later closely follow the O14-C4 BCPs of the excited state of OHBA, see Fig. 4b, this is not the case for the O12-C11 BCP of the excited OHBA. From this observation, it can be said that the substitution of either -OH or -OCH_3 in SA and MS respectively, affects the ellipticity of C11-O12 BCPs significantly compared with that of the C11-O12 BCPs in the OHBA molecule in the excited state. A possible reason, that in the excited state the ellipticity ε values of the C4-O14 BCPs of both SA and MS closely follow those of the corresponding value of OHBA, is that the substituent site is too far away to render any significant effect on the QTAIM properties at the site of the C4-O14 BCPs. A further point to note is that, for the excited state of the OHBA molecule the variation of ε with reaction pathway coordinate of the O14-C4 BCPs resembles a sine function; which is not the case for the ground state. A possible explanation is that the proton is coupling to the electronic charge density [65] with a higher level of responsiveness, corresponding to the smoother sinusoidal like variation of the ellipticity ε with reaction coordinate; the consequence is that ESIPT occurs more readily in the excited state of the OHBA molecule than in the other bonding environments, either the ground state of the OHBA molecule or even the excited SA and MS molecules. For an example of the proton coupling with the electronic charge density we compare the actual direction motion of the H15 nuclei moving from reaction coordinate '1' shown in Figs. 3b with the motion predicted by the $\underline{\mathbf{e}_2}$ eigenvector of the O14-H15 and O12—H15 BCPs of the structure with reaction pathway coordinate

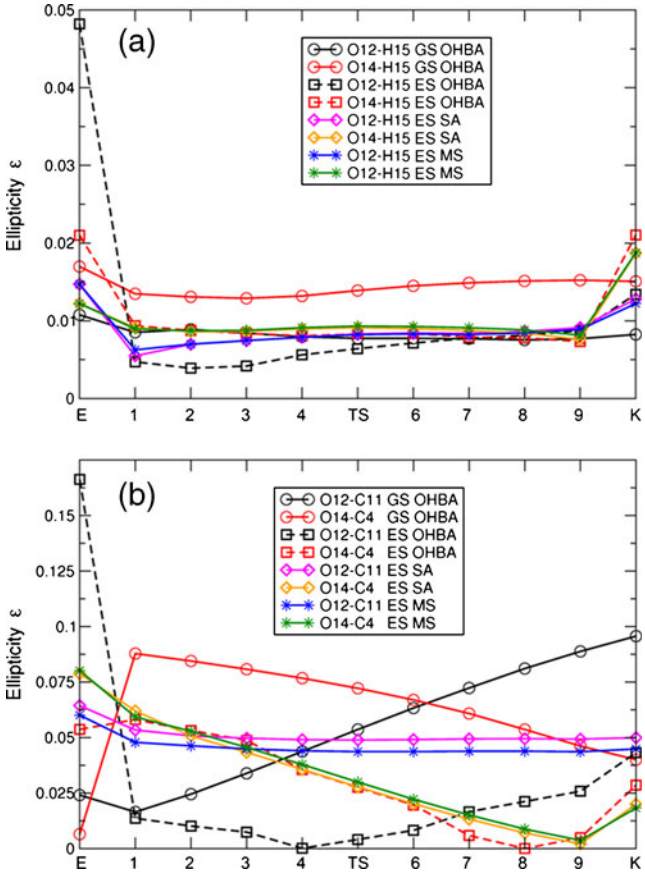

Fig. 4 The variation of ellipticity ε with reaction pathway coordinate of different O-H and C-O bonds in the ground and excited sates (mentioned as GS and ES, respectively). See Fig. 1 for atom numbering

'1'. The actual direction of motion of the H15 nuclei moving between reaction coordinates '1' and '2' is calculated to be [0.274, 0.961, 0.000], using the Cartesian axis specified in Fig. 3b. This can be compared to the $\underline{\mathbf{e_2}}$ eigenvectors [0.526, 0.850, 0.000] and [0.899, 0.439, 0.000] of the O14-H15 and O12—H15 BCPs determined from the structure with reaction pathway coordinate of '1'. Further, we see that the H15 nuclei will move inward in the plane of the molecule under a perturbing force in a direction specified by the directions of the $\underline{\mathbf{e_2}}$ eigenvectors of the stress tensor $\sigma(r_b)$. This finding is consistent with the *ab-initio* calculation results described in the previous sections.

The changing nature of the bonding during ESIPT: covalent and metallic character

From the expression to determine whether a BCP is shared shell or closed shell; $|\lambda_1|/\lambda_3 > 1$ and we see how this ratio changes for the O-H BCPs and C-O BCPs in Figs. 4S(a) and 4S(b) respectively, for the systems studied here. It can be seen that all the C-O BCPs have closed shell character in contrast to the O-H BCPs. The transition between OH sigma bond and hydrogen bond behavior occurs where the value of the ratio $|\lambda_1|/\lambda_3$ falls below 1. Referring back to the RCP-BCP paths in Fig. 3 for the OHBA molecule, this transition occurs when the H15 nuclei resides mid-way between the O12 and O14 nuclei at reaction coordinate '6', see Fig. 5d. At this cross over point, the values of $|\lambda_1|/\lambda_3$ are equal for the O12-H15 and O14-H15 BCPs and the RCP-BCP paths and molecular graph are rather symmetrical with respect to the H15 nuclei and the O12 and O14 nuclei.

In the SA and MS molecules, this cross-over point occurs at reaction pathway coordinates at the TS, the RCP-BCP paths and molecular graphs are again symmetrical with respect to the H15 nuclei and the O12 and O14 nuclei. From this, we see that there is a complete change in the chemical character of the O12-H15 and O14-H15 hydrogen bonds in the vicinity of the TS.

It can be seen for each point on the reaction pathway of the OHBA molecule in the ground and excited states that there is a cross-over in the covalent character $H(\mathbf{r}_b)$, given by Eq. 4, between the BCPs of the two OH bonds involved in the proton transfer pathway; O12-H15 and O14-H15, see Fig. 5S(a). This is also true for the O-H BCP pairs in the SA and MS molecules. The exchange of covalent character between the two O-H bonds participating in the proton transfer reaction is clearly evident, where the O14-H15 sigma bond becomes a hydrogen bond at the end of the reaction pathway, represented by the reaction pathway coordinates increasing from **E** → **K** and conversely, O12–H15, a hydrogen bond transforms into a sigma bond as the proton moves between O12 and O14. Coupling between adjacent OH sigma bonds and O—H hydrogen bonds has been observed before by one of us [38].

There is a very close correspondence between the values of $H(\mathbf{r}_b)$ for the equivalent OH bonds in the SA and MS molecules showing that changing the substituent from -OH to $-OCH_3$ has little effect on the $H(\mathbf{r}_b)$ values of the OH bonding. The $H(\mathbf{r}_b)$ values of the O12—H15 BCP of OHBA in the excited state closely follow the variation in the corresponding ground state parameter until the reaction pathway coordinate '6'. Beyond this point, the values of $H(\mathbf{r}_b)$ of the O12—H15 BCPs for the ground and excited states diverge. Then the excited state values of $H(\mathbf{r}_b)$ of the O12—H15 BCPs of OHBA switch to following the values of $H(\mathbf{r}_b)$ for the O12—H15 BCPs of SA and MS. This process also occurs for the value of $H(\mathbf{r}_b)$ for the OHBA molecule in the excited state O14–H15 BCP, although there is less similarity with the ground state values of $H(\mathbf{r}_b)$ in this case. This tighter coupling of the OHBA in the excited state values of $H(\mathbf{r}_b)$ with those in the SA and MS appears to happen also for the O14-C4 BCPs, shown in Fig. 5S(b), although to a relatively weaker extent. Strong coupling of the values of $H(\mathbf{r}_b)$ for the O14-C4 BCPs in the ground as well as in the excited states of OHBA molecule

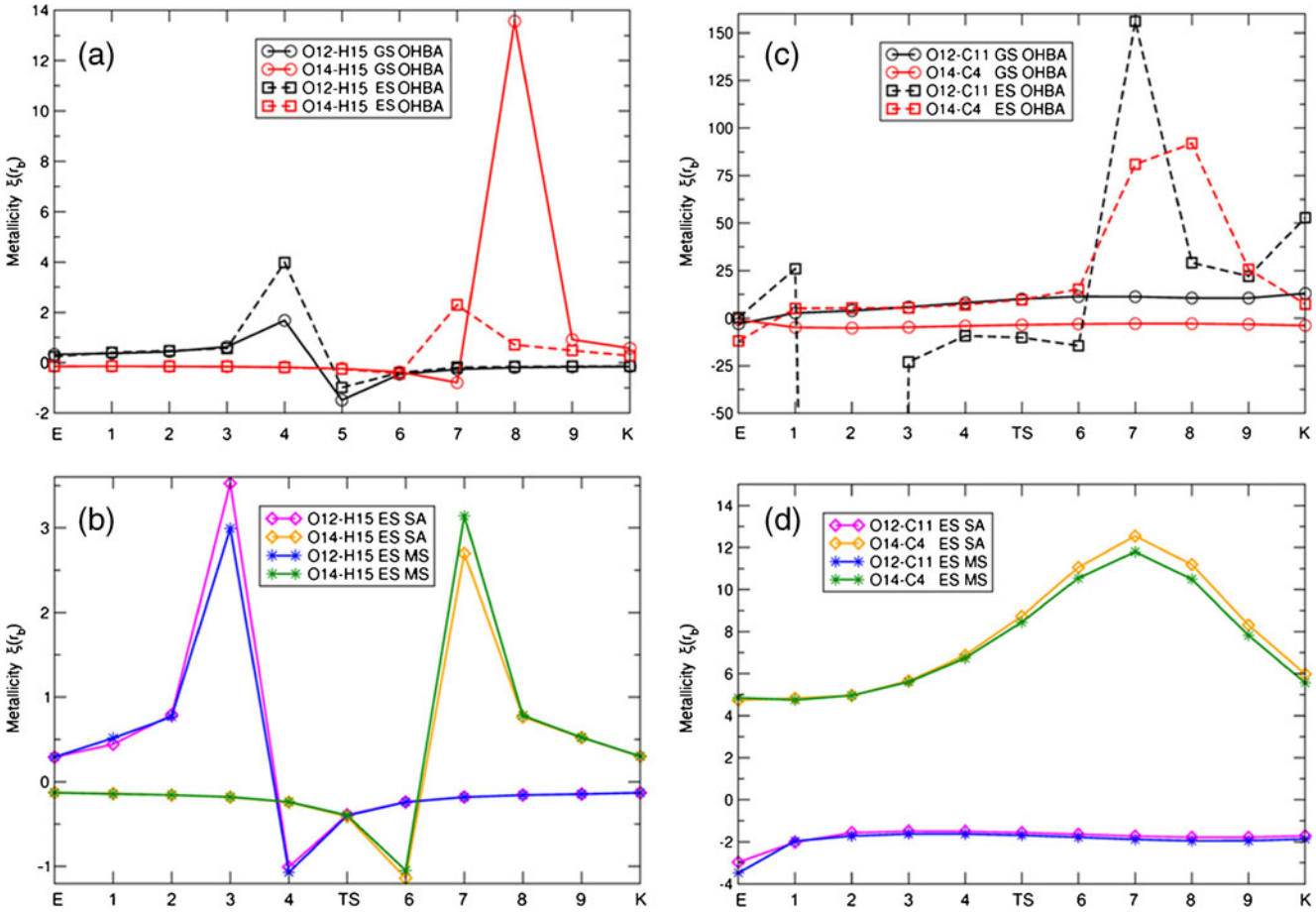

Fig. 5 The variation of metallicity $\xi(r_b)$ with reaction pathway coordinate of different O-H and C-O bonds in the ground and excited sates (mentioned as GS and ES, respectively). See Fig. 1 for atom numbering

are present and persist for most of the reaction pathway. The tighter correspondence in the excited state values of H($\mathbf{r}_b$) with the O14-C4 BCPs compared with those of the O12-C11 BCPs in the SA and MS may again be due to some kind of coupling effects of O12-C11 BCPs being hindered by the proximity of the substituent group. There is again an exchange of the values of H($\mathbf{r}_b$) for the pairs of OC BCPs in each molecule but further along the reaction pathway than is the case for the OH BCPs, i.e., the values of H($\mathbf{r}_b$) for the O12-C11 and O14-C4 BCPs in both the SA and MS molecules cross-over at reaction coordinate at just over '6' as compared with over '7' and just under '6' for the OC for the ground state and excited states of the OHBA molecule respectively. This shows that for the values of H($\mathbf{r}_b$) in the O12-C11 and O14-C4 BCPs differences in the ground state and excited states for the OHBA molecule are larger than for the OH BCPs.

Finally, we will compare the metallicity $\xi(r_b)$, from Eq. 5, of the four BCPs that are mostly involved with the proton transfer reaction, i.e., the BCPs of the O12-H15, O14-H15, C11-O12 and C4-O14 bonds of OHBA in the ground and excited states before comparing the effect of changing the substituent group in the cases of SA and MS.

The proton H15 in the OHBA molecule in the ground state and excited state moves between O12 and O14, it initially forms a sigma bond with O14 then moves toward O12 to form a sigma bond with O12 and a hydrogen bond with O14, this much is already ascertainable without using QTAIM. However, with QTAIM, we see that the as the proton moves from the reaction pathway coordinate '2' between O12 and O14, the hydrogen bonding becomes increasingly metallic in character. The O12-H15 and O14-H15 BCPs for the OHBA molecule in the ground state are determined to have maximally metallic hydrogen bonds at reaction pathway coordinates of '4' and '8', respectively. There is a metallic to non-metallic transition for the O12-H15 to O14–H15 BCPs, both the ground and excited states of the OHBA molecule, between reaction pathway coordinates of '4 'and the TS, see Fig. 5. On the other hand, non-metallic to metallic effect occurs for the formation of the O14-H15 bond at a reaction pathway coordinate of '8' for the ground state and '7' for the excited state. While comparing the ground and excited states of OHBA, it is seen that the ESIPT reaction is non-symmetrical with respect to the maximum metallicity $\xi(r_b)$ of the hydrogen bonds O12–H15

and O14–H15 BCPs. There is a large negative spike at a value of −3000 at a reaction pathway coordinate of '2' for the O12-C11 BCP for OHBA molecule in the excited state, this is due to an extremely low value of the Laplacian.

Examination of the metallicity $\xi(r_b)$ for O12–H15 and O14–H15 BCPs for the SA and MS molecules shows the proton transfer reaction to be more symmetrical in these cases as compared with OHBA, see Fig. 5a, b. The MS molecule possessing the most symmetrical proton transfer reaction with respect to the metallicity of O12···H15 and O14···H15 bond BCPs, although the metallic behaviors of both the OH and CO BCPs of the SA and MS molecules are still distinguishable. From this symmetry, we can see that the TS for the OH bonds both in the SA and MS molecules is preceded by a large spike in the metallicity $\xi(r_b)$ of O12-H15 then immediately followed by a negative value of the metallicity $\xi(r_b)$ before the cross-over with the metallicity $\xi(r_b)$ values of O14-H15 BCPat the TS.

For the C11-O12 and O14-C4 BCPs of the OHBA molecule, the metallic behavior of the ground state contrasts strongly with the excited state as can be seen from Fig. 5c, d respectively, where both the C11-O12 and O14-C4 BCPs in the excited state display very large peaks in the metallicity compared with the corresponding values of $\xi(r_b)$ for the BCPs in the ground state. In fact, the O14-C4 BCPs of the OHBA molecule in the ground state possess no metallicity. In the O12-C11 BCPs in both the SA and MS molecules where, in each case, the BCP possess no metallicity, see Fig. 5c. For the SA and MS molecules there are peaks in the values of the $\xi(r_b)$ of the O14-C4 BCPs and O14-H15 BCPs and that both occur at the reaction pathway coordinate of '7', see Fig. 5b, d respectively. An explanation of this could be that the O14-C4 and O14-H15 bonds are coupling since they are adjacent to one another.

Conclusions

The ESIPT process in OHBA and its derivatives, MS and SA, was investigated completely based on the analysis of the structural parameters, rate constant, energies, dipole moments of different structures along the reaction path. The stability reversal of the phototautomers in the excited state suggested that these molecules had large possibility to undergo ESIPT, which was further demonstrated by a low energy barrier during the process. ESIPT rate calculation using simple transition state theory can qualitatively predict the trend in different systems; however, consideration of over-barrier process seems indispensable to match the calculated values with experimental measurements, particularly for highly asymmetric system like OHBA. We have also used QTAIM in this first exploration of excited state proton transfer phenomena and find that QTAIM is able to provide new insights into the changes in bonding character during the process of ESIPT. This is possible as we are able to quantify the changes in the bond stability, covalent and metallic character of the bonding on a bond-by-bond basis throughout the ESIPT path. QTAIM seems to be able predict the onset of the TS by the occurrence of a drastic change in the QTAIM parameters like metallicity $\xi(r_b)$ and ellipticity ε and abrupt changes in the bonding character $|\lambda_1|/\lambda_3$. The process of excitation of the OHBA molecule induces metallic character in the O14-C4 BCP relative to the ground state and increases the metallicity in the O12-C11 BCP by an order of magnitude. In addition, excitation of the OHBA molecule reduces the bond ellipticities in the OH and OC BCPs, thus providing evidence of facilitating the motion of the H15 nuclei. In addition, we can predict the direction that the H15 atom will move by comparison of the actual direction that the H15 atom moved with the O14-H15 and O12–H15 BCP $\underline{\mathbf{e}_2}$ eigenvectors of the stress tensor and suggests that this could be a useful area of further investigation. The use of the QTAIM parameters for ESIPT in these systems raises some interesting questions like why the O12-C11 BCPs possess a higher degree of metallicity than the O12-H15 or O14-H15 BCPs in these molecules. Another question is why the substitution by -OH and -OCH3, in SA and MS respectively, does remove the metallic character of the adjacent O12-C11 BCPs. Further work on similar systems both in the ground and excited states that contain an intra-molecular hydrogen bond but do not undergo ESIPT, e.g, 1-hydroxy fluorenone (HOF) may help with understanding such issues.

Acknowledgments Thanks are due to Board of Research in Nuclear Sciences (BRNS) and Council of Scientific and Industrial Research (CSIR), Govt. of India for providing financial assistance to SM [project no. 2009/37/26/BRNS/1900] and AKC [project No. 01(2494)/11/EMR-II], respectively. The Hundred Talents Foundation of Hunan Province is gratefully acknowledged for the support of SJ and SRK.

References

1. Weller A (1961) Fast reactions of excited molecules. Prog React Kinet 1:189–214
2. Weller A (1957) Protolytische reaktionen des angeregten acridins. Zeitschrift fur Elektrochemie 61(8):956–961
3. Weller A (1955) Über die Fluoreszenz der Salizylsäure und verwandter Verbindungen. Naturwissenschaften 42(7):175–176. doi:10.1007/BF00595299
4. Tang KC, Chang MJ, Lin TY, Pan HA, Fang TC, Chen KY, Hung WY, Hsu YH, Chou PT (2011) Fine tuning the energetics of excited-state intramolecular proton transfer (ESIPT): white light generation in a single ESIPT system. J Am Chem Soc 133 (44):17738–17745. doi:10.1021/ja2062693
5. Xu S, Shao Y, Ma K, Cui Q, Liu G, Wu F, Li M (2011) Fluorescence light-up recognition of DNA nucleotide based on selective abasic site binding of an excited-state intramolecular proton transfer probe. Analyst 136(21):4480–4485. doi:10.1039/C1AN15652G

6. Kwon JE, Park SY (2011) Advanced organic optoelectronic materials: harnessing excited-state intramolecular proton transfer (ESIPT) process. Adv Mater 23(32):3615–3642. doi:10.1002/adma.201102046
7. Shvadchak VV, Falomir-Lockhart LJ, Yushchenko DA, Jovin TM (2011) Specificity and kinetics of α-synuclein binding to model membranes determined with fluorescent excited state intramolecular proton transfer (ESIPT) probe. J Biol Chem 286(15):13023–13032. doi:10.1074/jbc.M110.204776
8. Shono H, Ohkawa T, Tomoda H, Mutai T, Araki K (2011) Fabrication of colorless organic materials exhibiting white luminescence using normal and excited-state intramolecular proton transfer processes. ACS Appl Mater Interfaces 3(3):654–657. doi:10.1021/am200022z
9. Kerkines ISK, Petsalakis ID, Theodorakopoulos G, Rebek J (2010) Excited-state intramolecular proton transfer in hydroxyoxime-based chemical sensors. J Phys Chem A 115(5):834–840. doi:10.1021/jp1088433
10. Zhao J, Ji S, Chen Y, Guo H, Yang P (2011) Excited state intramolecular proton transfer (ESIPT): from principal photophysics to the development of new chromophores and applications in fluorescent molecular probes and luminescent materials. Phys Chem Chem Phys. doi:10.1039/C2CP23144A
11. Sun W, Li S, Hu R, Qian Y, Wang S, Yang G (2009) Understanding solvent effects on luminescent properties of a triple fluorescent ESIPT compound and application for white light emission. J Phys Chem A 113(20):5888–5895. doi:10.1021/jp900688h
12. Miyasaka T, Koyama K, Itoh I (1992) quantum conversion and image detection by a bacteriorhodopsin-based artificial photoreceptor. Science 255(5042):342–344. doi:10.1126/science.255.5042.342
13. Ernsting NP, Nikolaus B (1986) Dye-laser pulse shortening by transient absorption following excited-state intramolecular proton transfer. Appl Phys B 39(3):155–164. doi:10.1007/BF00697413
14. Chou P-T, Studer SL, Martinez ML (1991) Practical and convenient 355-nm and 337-nm sharp-cut filters for multichannel raman spectroscopy. Appl Spectrosc 45(3):513–515
15. Sengupta PK, Kasha M (1979) Excited state proton-transfer spectroscopy of 3-hydroxyflavone and quercetin. Chem Phys Lett 68 (2–3):382–385. doi:10.1016/0009-2614(79)87221-8
16. Guo Z-Q, Chen W-Q, Duan X-M (2012) Seven-membered ring excited-state intramolecular proton-transfer in 2-benzamido-3-(pyridin-2-yl)acrylic acid. Dye Pigment 92(1):619–625. doi:10.1016/j.dyepig.2011.06.004
17. Formosinho SJ, Arnaut LG (1993) Excited-state proton transfer reactions II. Intramolecular reactions. J Photochem Photobiol A 75 (1):21–48. doi:10.1016/1010-6030(93)80158-6
18. El-Sayed MA, Barbara P, Nicol M (1991) Michael Kasha - editorial, biographical sketch, summary of research contributions, research associates, and publications list. J Phys Chem 95 (25):10215–10220. doi:10.1021/j100178a001
19. Zhao G-J, Han K-L (2011) Hydrogen bonding in the electronic excited state. Acc Chem Res. doi:10.1021/ar200135h
20. Kijak M, Nosenko Y, Singh A, Thummel RP, Waluk J (2007) Mode-selective excited-state proton transfer in 2-(2‘-Pyridyl)pyrrole isolated in a supersonic jet. J Am Chem Soc 129(10):2738–2739. doi:10.1021/ja068109f
21. Rambaud C, Oppenländer A, Pierre M, Trommsdorff HP, Vial J-C (1989) Tunneling dynamics of delocalized protons in benzoic acid dimers: a study of the temperature dependence by time and frequency domain optical spectroscopy. Chem Phys 136(2):335–347. doi:10.1016/0301-0104(89)80057-6
22. Shida N, Barbara PF, Almlöf JE (1989) A theoretical study of multidimensional nuclear tunneling in malonaldehyde. J Chem Phys 91(7):4061–4072. doi:10.1063/1.456836
23. Schwartz BJ, Peteanu LA, Harris CB (1992) Direct observation of fast proton transfer: femtosecond photophysics of 3-hydroxyflavone. J Phys Chem 96(9):3591–3598. doi:10.1021/j100188a009
24. Yu W-S, Cheng C-C, Cheng Y-M, Wu P-C, Song Y-H, Chi Y, Chou P-T (2003) Excited-state intramolecular proton transfer in five-membered hydrogen-bonding systems: 2-pyridyl pyrazoles. J Am Chem Soc 125(36):10800–10801. doi:10.1021/ja035382y
25. Nagaoka S, Teramae H, Nagashima U (2009) Computational study of excited-state intramolecular-proton-transfer of o-hydroxybenzaldehyde and its derivatives. Bull Chem Soc Jpn 82(5):570–573. doi:10.1246/bcsj.82.570
26. Scheiner S (2000) Theoretical studies of excited state proton transfer in small model systems. J Phys Chem A 104(25):5898–5909. doi:10.1021/jp000125q
27. Schriever C, Lochbrunner S, Riedle E (2009) Influence of the environment on reaction dynamics: excited state intramolecular proton transfer in the gas phase and in solution. In: Corkum P, Silvestri S, Nelson KA, Riedle E, Schoenlein RW (eds) Ultrafast phenomena XVI. Springer, Heidelberg, pp 508–510
28. Frisch M, Trucks G, Schlegel H et al. (2004) Gaussian 03, Revision D.01. Gaussian Inc, Wallingford
29. Laidler KJ (2004) Chemical kinetics, 3rd edn. Pearson Education, New Delhi
30. Johnston HS, Heicklen J (1962) Tunnelling corrections for unsymmetrical Eckart potential energy barriers. J Phys Chem 66(3):532–533. doi:10.1021/j100809a040
31. Jogeshwari Devi K, Chandra AK (2011) Kinetics and thermochemistry of the gas-phase reactions of 4-ethylpyridine with OH radical: a DFT study. Comput Theory Chem 965(2–3):268–274. doi:10.1016/j.comptc.2010.12.015
32. Bader RFW (1994) Atoms in molecules: a quantum theory. Oxford University Press, USA
33. Jenkins S, Heggie MI (2000) Quantitative analysis of bonding in 90° partial dislocation in diamond. J Phys Condens Matter 12 (49):10325–10333. doi:10.1088/0953-8984/12/49/3
34. Jenkins S (2002) Direct space representation of metallicity and structural stability in SiO solids. J Phys Condens Matter 14 (43):10251–10263. doi:10.1088/0953-8984/14/43/321
35. Koch U, Popelier PLA (1995) Characterization of C-H-O hydrogen bonds on the basis of the charge density. J Phys Chem 99 (24):9747–9754. doi:10.1021/j100024a016
36. Jenkins S, Morrison I (1999) Characterization of various phases of ice on the basis of the charge density. J Phys Chem B 103 (50):11041–11049. doi:10.1021/jp992655w
37. Cremer D, Kraka E (1984) A description of the chemical bond in terms of local properties of electron density and energy. Croat Chem Acta 57:1265–1287
38. Jenkins S, Morrison I (2000) The chemical character of the intermolecular bonds of seven phases of ice as revealed by *ab initio* calculation of electron densities. Chem Phys Lett 317(1–2):97–102. doi:10.1016/S0009-2614(99)01306-8
39. Isaacs ED, Shukla A, Platzman PM, Hamann DR, Barbiellini B, Tulk CA (1999) Covalency of the hydrogen bond in ice: a direct x-ray measurement. Phys Rev Lett 82(3):600–603. doi:10.1103/PhysRevLett.82.600
40. Pauling L (1948) The nature of the chemical bond and the structure of molecules and crystals: an introduction to modern structural chemistry. Cornell University Press etc, Ithaca
41. Silvi B, Gatti C (2000) Direct space representation of the metallic bond. J Phys Chem A 104(5):947–953. doi:10.1021/jp992784c
42. Silvi B, Savin A (1994) Classification of chemical bonds based on topological analysis of electron localization functions. Nature 371 (6499):683–686. doi:10.1038/371683a0
43. Wang Y-G, Wiberg KB, Werstiuk NH (2007) Correlation effects in EOM-CCSD for the excited states: evaluated by AIM localization

index (LI) and delocalization index (DI). J Phys Chem A 111 (18):3592–3601. doi:10.1021/jp067579t
44. Bhatt RN, Sachdev S (1986) Excited states and the metal-insulator transition in monovalent systems. Phys Rev B 34(5):3520–3523. doi:10.1103/PhysRevB.34.3520
45. Jenkins S, Kirk SR, Cote AS, Ross DK, Morrison I (2003) Dependence of the normal modes on the electronic structure of various phases of ice as calculated by *ab initio* methods. Can J Phys 81(7):225–231
46. Jones H, Curl RF Jr (1972) Microwave spectrum of salicyl aldehyde: structure of the hydrogen bond. J Mol Spectrosc 42(1):65–74. doi:10.1016/0022-2852(72)90144-0
47. Sundaralingam M, Jensen LH (1965) Refinement of the structure of salicylic acid. Acta Cryst 18:1053–1058. doi:10.1107/S0365110X65002517
48. Nagaoka S, Hirota N, Sumitani M, Yoshihara K (1983) Investigation of the dynamic processes of the excited states of o-hydroxybenzaldehyde and o-hydroxyacetophenone by emission and picosecond spectroscopy. J Am Chem Soc 105(13):4220–4226. doi:10.1021/ja00351a016
49. Morgan MA, Orton E, Pimentel GC (1990) Characterization of ground and electronically excited states of o-hydroxybenzaldehyde and its non-hydrogen-bonded photorotamer in 12 K rare gas matrixes. J Phys Chem 94(20):7927–7935. doi:10.1021/j100383a034
50. Law KY, Shoham J (1994) Photoinduced proton transfers in methyl salicylate and methyl 2-hydroxy-3-naphthoate. J Phys Chem 98 (12):3114–3120. doi:10.1021/j100063a013
51. Lahmani F, Zehnacker-Rentien A (1997) Effect of substitution on the photoinduced intramolecular proton transfer in salicylic acid. J Phys Chem A 101(35):6141–6147. doi:10.1021/jp9712516
52. Sobolewski AL, Domcke W (1998) *Ab initio* study of excited-state intramolecular proton dislocation in salicylic acid. Chem Phys 232 (3):257–265. doi:10.1016/S0301-0104(98)00110-4
53. Mitra S, Tamai N (1998) Femtosecond spectroscopic study on photochromic salicylideneaniline. Chem Phys Lett 282(5–6):391–397. doi:10.1016/S0009-2614(97)01279-7
54. de Klerk JS, Bader AN, Ariese F, Gooijer C (2009) High-resolution fluorescence studies on excited-state intra- and intermolecular proton transfer. In: Geddes CD, Lakowicz JR (eds) Reviews in fluorescence 2007. Springer, New York, pp 271–298. doi:10.1007/978-0-387-88722-7_12
55. Truong TN, Truhlar DG (1990) *Ab initio* transition state theory calculations of the reaction rate for OH + CH4 → H2O + CH3. J Chem Phys 93(3):1761–1769. doi:10.1063/1.459103
56. Subotnik JE (2011) Communication: configuration interaction singles has a large systematic bias against charge-transfer states. J Chem Phys 135(7):071104–071104–4. doi: 10.1063/1.3627152
57. Mitra S, Das R, Bhattacharyya SP, Mukherjee S (1997) Energetic and dynamic aspects of intramolecular proton transfer in 4-Methyl-2,6-diformylphenol: a detailed analysis with AM1 potential energy surfaces. J Phys Chem A 101(3):293–298. doi:10.1021/jp961560g
58. Migani A, Blancafort L, Robb MA, DeBellis AD (2008) An extended conical intersection seam associated with a manifold of decay paths: excited-state intramolecular proton transfer in o-hydroxybenzaldehyde. J Am Chem Soc 130(22):6932–6933. doi:10.1021/ja8013924
59. Lochbrunner S, Schultz T, Schmitt M, Shaffer JP, Zgierski MZ, Stolow A (2001) Dynamics of excited-state proton transfer systems via time-resolved photoelectron spectroscopy. J Chem Phys 114(6):2519–2522. doi:10.1063/1.1345876
60. Herek JL, Pedersen S, Bañares L, Zewail AH (1992) Femtosecond real–time probing of reactions. IX. Hydrogen–atom transfer. J Chem Phys 97(12):9046–9061. doi:10.1063/1.463331
61. Johnston HS (2007) Large tunnelling corrections in chemical reaction rates. In: Prigogine I (ed) Advances in chemical physics 3. Wiley, pp 131–170. doi: 10.1002/9780470143490.ch4
62. Johnston HS, Parr C (1963) Activation energies from bond energies. I. Hydrogen transfer reactions. J Am Chem Soc 85(17):2544–2551. doi:10.1021/ja00900a002
63. Maity DK, Bhattacharyya SP (1990) The behavior of quantum chemical bond order in the vicinity of a saddle point on the reaction path. J Am Chem Soc 112(8):3223–3225. doi:10.1021/ja00164a060
64. Keith TA (2010) AIMAll version 10.09.12. http://aim.tkgristmill.com.
65. Ayers PW, Jenkins S (2009) An electron-preceding perspective on the deformation of materials. J Chem Phys 130(15):154104–154104–11. doi: 10.1063/1.3098140